

International Journal of Modern Physics C
 © World Scientific Publishing Company

VALIDATION EXPERIMENTS FOR LBM SIMULATIONS OF ELECTRON BEAM MELTING

REGINA AMMER* and ULRICH RÜDE†

*Department of Computer Science 10 System Simulation, University of Erlangen-Nuremberg,
 Cauerstr. 11, 91058 Erlangen, Germany*

**regina.ammer@fau.de*

†*ulrich.ruede@fau.de*

MATTHIAS MARKL*, VERA JÜCHTER† and CAROLIN KÖRNER‡

*Chair of Metals Science and Technology, University of Erlangen-Nuremberg,
 Martensstr. 5, 91058 Erlangen, Germany*

**matthias.markl@fau.de*

†*vera.juechter@ww.uni-erlangen.de*

‡*carolin.koerner@ww.uni-erlangen.de*

Received Day Month Year

Revised Day Month Year

This paper validates 3D simulation results of electron beam melting (EBM) processes comparing experimental and numerical data. The physical setup is presented which is discretized by a three dimensional (3D) thermal lattice Boltzmann method (LBM). An experimental process window is used for the validation depending on the line energy injected into the metal powder bed and the scan velocity of the electron beam. In the process window the EBM products are classified into the categories, porous, good and swelling, depending on the quality of the surface. The same parameter sets are used to generate a numerical process window. A comparison of numerical and experimental process windows shows a good agreement. This validates the EBM model and justifies simulations for future improvements of EBM processes. In particular numerical simulations can be used to explain future process window scenarios and find the best parameter set for a good surface quality and dense products.

Keywords: 3D thermal lattice Boltzmann method; free surface; electron beam melting; validation experiments.

PACS Nos.: 11.25.Hf, 123.1K

1. Introduction

Electron beam melting (EBM) is an additive manufacturing method used to produce complex metallic structures layer by layer from metal powder¹. EBM opens new opportunities in many industries, ranging from aircraft manufacturers to producers of medical implants. However, until now the parts cannot be manufactured at sufficient speed to make them economically viable for any but specific very high

2 *Regina Ammer, Matthias Markl, Vera Jüchter, Carolin Körner, Ulrich Rüde*

value applications. In order to accelerate the building process and improve the accuracy a better understanding of the beam-powder interaction is necessary. This can be gained by 3D simulations of the process.

Based on the work of Körner et al.² we use a 3D thermal LBM for the discretization for the EBM processes. This model includes hydrodynamic effects, like melt flow, capillarity and wetting, as well as thermal effects, like absorption of the beam energy, melting and solidification. Detailed information for parallel, optimized 3D absorption algorithms is found in ³ and the description of the modeling aspects, e.g., the generation of the Ti-Al6-V4 powder particles is given in ⁴. The implementation of the model is embedded in the WALBERLA framework (widely applicable lattice Boltzman solver from Erlangen) which is a lattice Boltzmann based fluid flow solver with highly parallelized kernels ^{5,6}. In ⁴ basic validation examples are already shown, like the test of the Stefan problem as benchmark for the simulation of solid-liquid phase transition, and modest EBM process examples, e.g., the melting of a spot regarding the interaction of powder particles and electron beam. In this paper we extend the validation examples focusing on the EBM processes, e.g. hatching scenarios, and compare the numerical results with experimental data. These numerical results demonstrate the good potential of the thermal LBM approach to understand and predict complex processes like the EBM depending on thermodynamic as well as on fluid dynamic phenomena.

The remainder of the paper is organized as follows: Section 2 describes the 3D thermal LBM used for the simulation of the EBM process. The next section defines line energy, scan velocity, porosity and swelling before showing the experimental process window. Subsequently, the generation of the numerical process window is described, shown and compared with the experimental one. Section 4 concludes the validation experiments and outlines future research topics.

2. Numerical methods

Based on the lattice Boltzmann equation the isothermal lattice Boltzmann method (LBM) is introduced by ⁷ as an improvement of its predecessor, the lattice gas automata (LGA) ⁸. LBM is an alternative, mesoscopic approach for the numerical solution of the Navier-Stokes equations ⁹ and can be parallelized easier than other traditional CFD methods whose computation is based on the conservation of macroscopic quantities. LBM has also less computational storage and work requirements than molecular dynamic methods which consider microscopic physics.

Thermal LB methods are classified into three categories: the multispeed LBM ^{10,11}, the double-distribution or multidistribution approach ^{12,13,14} and hybrid approach where the scalar temperature equation is solved by finite differences or finite volume methods ¹⁵. The multispeed LBM can be seen as an extension of the isothermal LBM where the equilibrium distribution function depends also on the temperature and has higher nonlinear velocity terms. This method suffers from numerical instabilities which have to be stabilized as it is shown in ¹⁶. An additional

disadvantage is that only one Prandtl number can be simulated by multispeed LBM which limits the range of applications. The multidistribution LBM overcomes these drawbacks using a separate distribution function for the temperature field.

For the simulation of the EBM process a thermal two-distribution LBM is used which is described followed by the treatment of the free surface boundary condition.

2.1. 3D thermal lattice Boltzmann method

The model for the EBM process is based on the work of Körner et al. in ² where a 2D thermal LBM is discussed. The idea of LBM is solving the Boltzmann equation in the hydrodynamic limit for a particle distribution function (pdf) in the physical momentum space. This pdf $f(\mathbf{x}, \mathbf{v}, t)$ indicates the probability of finding a particle with the macroscopic velocity $\mathbf{v}(\mathbf{x}, t)$ at position \mathbf{x} and time t . For the thermal LBM a second pdf set $h(\mathbf{x}, \mathbf{v}, t)$ is used for the numerical solution of the temperature field. The collision operator is approximated by the BGK-collision operator ^{17,11},

$$\Omega_f = -\frac{1}{\tau_f}(f - f^{eq}), \quad \Omega_h = -\frac{1}{\tau_h}(h - h^{eq}), \quad (1)$$

where f^{eq} and h^{eq} denote the Maxwell equilibrium distribution ¹⁹. τ_f is the relaxation time related to the viscosity ν of the fluid and given by $\nu = c_s^2 \Delta t (\tau_f - 0.5)$ with the lattice speed of sound $c_s^2 = \frac{\Delta x^2}{3\Delta t^2}$. τ_h belongs to the second pdf set h_i and there exists the relation to the thermal diffusivity $k = c_s^2 \Delta t (\tau_h - 0.5)$.

The D3Q19 stencil is used to discretize the microscopic space, i.e., a finite set of 19 discrete velocities \mathbf{e}_i and lattice weights ω_i are given ¹⁹. The Maxwell equilibrium distribution is discretized by a Taylor series expansion ²⁰ and is given by,

$$f_i^{eq}(\mathbf{x}, t) = \omega_i \rho \left[1 + \frac{(\mathbf{e}_i \cdot \mathbf{u})}{c_s^2} + \frac{(\mathbf{e}_i \cdot \mathbf{u})^2}{2c_s^4} - \frac{\mathbf{u}^2}{2c_s^2} \right], \quad h_i^{eq}(\mathbf{x}, t) = \omega_i E \left[1 + \frac{(\mathbf{e}_i \cdot \mathbf{u})}{c_s^2} \right] \quad (2)$$

where \mathbf{u} denotes the velocity of the liquid. It is sufficient to use a linearized equilibrium distribution function h_i^{eq} for the temperature field. The macroscopic quantities density ρ , momentum $\rho \mathbf{u}$ and energy density E are computed in the following way,

$$\rho = \sum_i f_i, \quad \rho \mathbf{u} = \sum_i \mathbf{e}_i f_i, \quad E = \sum_i h_i. \quad (3)$$

Both pdf sets are one-way coupled by the velocity of the fluid \mathbf{u} which is used for the computation of h_i^{eq} . The discretization of the EBM process by a 3D coupled-thermal LBGK ⁴ can be written in a stream-collide algorithm,

$$\text{streaming} \begin{cases} f'_i(\mathbf{x} + \mathbf{e}_i \Delta t, t + \Delta t) & = f_i(\mathbf{x}, t) \\ h'_i(\mathbf{x} + \mathbf{e}_i \Delta t, t + \Delta t) & = h_i(\mathbf{x}, t), \end{cases} \quad (4)$$

$$\text{collide} \begin{cases} f_i(\mathbf{x}, t + \Delta t) & = f'_i(\mathbf{x}, t + \Delta t) + \frac{1}{\tau_f}(f_i^{eq}(\rho, \mathbf{u}) - f_i(\mathbf{x}, t + \Delta t)) + F_i \\ h_i(\mathbf{x}, t + \Delta t) & = h'_i(\mathbf{x}, t + \Delta t) + \frac{1}{\tau_h}(h_i^{eq}(E, \mathbf{u}) - h_i(\mathbf{x}, t + \Delta t)) + \Phi_i, \end{cases} \quad (5)$$

4 Regina Ammer, Matthias Markl, Vera Jüchter, Carolin Körner, Ulrich Rude

where F_i denotes an external force term, e.g., gravity, and Φ_i is the energy injected into the system by the electron beam,

$$F_i = \omega_i \rho \left[\frac{(\mathbf{e}_i - \mathbf{u})}{c_s^2} + \frac{(\mathbf{e}_i \cdot \mathbf{u})\mathbf{e}_i}{c_s^4} \right] \cdot \mathbf{g}, \quad \Phi_i(\mathbf{x}, t) = \omega_i E_b(\mathbf{x}, t), \quad (6)$$

where E_b denotes the energy of the electron beam. Detailed information how the beam energy and absorption are computed is given in ^{3,4}. Next, the free surface boundary condition is outlined.

2.2. Free surface lattice Boltzmann method

Körner et al. introduce in ²¹ a volume-of-fluid based free surface lattice Boltzmann approach. This method neglects the gas phase and works completely on the liquid phase assuming that the liquid phase covers the behavior of the flow completely. In order to ensure mass and momentum conservation a boundary condition is imposed at the interface which separates liquid and gas phase. More information regarding the free surface boundary condition used for this EBM model can be found in ⁴.

3. Validation experiments

The following validation experiments do not only cover particular aspects as the solid-liquid phase transition or only concentrate on qualitative accordance but consider also the complete EBM process in a quantitative way.

3.1. Definitions and experimental setup

We use the following experimental setup for the validation experiments. A cuboid of size (15x15x10) mm³ is generated by hatching the Ti-Al6-V4 powder particles layer by layer (compare the red arrows in Fig. 1). The hatching differs by line energy and scan velocity of the electron beam. The line energy is defined by,

$$E_L = \frac{U \cdot I}{v_{\text{scan}}} = \frac{P_{\text{beam}}}{v_{\text{scan}}}, \quad (7)$$

where U denotes the acceleration voltage in [V], I the current in [A] and v_{scan} the scan velocity in [$\frac{\text{m}}{\text{s}}$] of the electron beam. The parameter set (E_L, v_{scan}) defines the electron beam. The quality of EBM products is classified into three categories, namely porous, good and swelling. Good samples have a smooth surface and a relative density higher than 99.5%. If the temperature during the process is too high swelling can occur and the dimensional accuracy cannot be guaranteed. On the other side, if the line energy is too low and the relative density is smaller than 99.5%, then the sample is porous (cf. Fig. 2). Next, a experimental

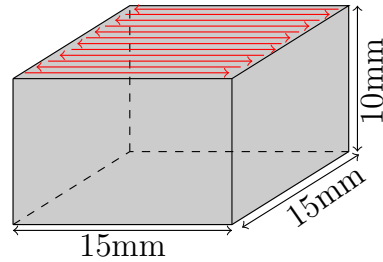


Fig. 1. Experimental setup.

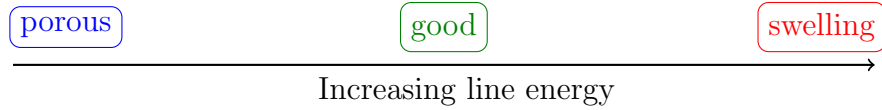


Fig. 2. Categories of samples.

process window is shown in Fig. 3 which is compared with numerical simulation results.

3.2. Experimental data

Fig. 3 shows the quality of samples with different line energies in $[\frac{\text{kJ}}{\text{m}}]$ and scan velocities in $[\frac{\text{m}}{\text{s}}]$ of the electron beam. The red circles stand for a porous parameter

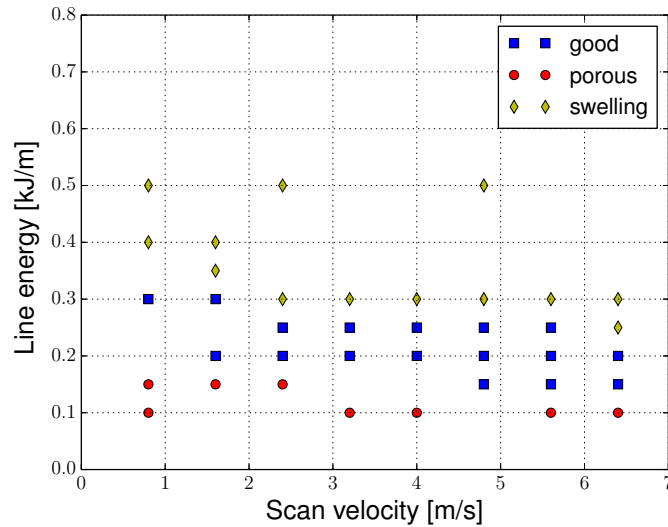


Fig. 3. Process window of experimental data. Built temperature 1000 K, line offset $100 \mu\text{m}$, layer thickness $50 \mu\text{m}$, focused electron beam.

set, the blue squares for an optimal, good parameter set and the yellow rhombus for a sample where swelling occurs because of too high temperatures at the surface. It can be observed that the higher the scan velocity the lower the embedded line energy has to be to get an optimal sample result.

3.3. Numerical results

We validate our 3D numerical EBM model against these experimental data of Fig. 3. Because of the high computational cost of the 3D simulations we only model the hatching of one powder layer instead of the multiple layers.

One simplified scenario for the exemplary parameter set of $(3.2 \frac{\text{m}}{\text{s}}, 0.2 \frac{\text{J}}{\text{m}})$ does already require 8 compute nodes of LIMA^a for 4 wall clock hours. LIMA is the compute cluster where all 3D simulations are done. However, this simplification is in good agreement with the situation expected for the full setup as it will be shown in this Section.

We also minimize the simulated powder particle layer, i.e., we focus only a rectangular powder layer and have seven hatching lines (cf. Fig. 4). Thus, a beam offset per layer is defined where the electron beam is on but outside the simulated powder particle bed.

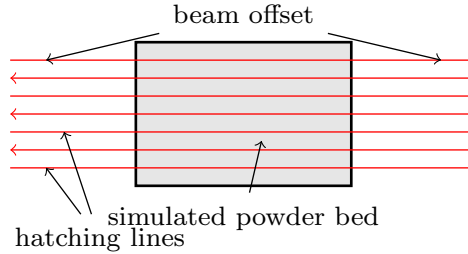


Fig. 4. Sketch of simulation scenario.

In Fig. 5 the quality of the numerical experiments with different line energy and scan velocity is shown. In order to determine if the numerical sample is porous the relative density of the sample is measured and if it is less than 99.5% the sample is porous. The definition of numerical swelling is more difficult. Our model does not include evaporation and thus no evaporation pressure. Hence, numerical swelling effects cannot occur. We have to find another way how we can determine regions numerically where swelling exists experimentally. Therefore, we use the numerical computed temperature which is higher than in real EB melting processes because the cooling effect during the process of evaporation is missing. Furthermore, numerical artefacts cause outliers in the temperature field. In order to overcome these numerical influences we use an averaging process for the temperature values. If these averaged values are still higher than 7500 K we assume that swellings occur in the experimental setup.

In comparison with the experimental data in Fig. 3 it is observed that all porous samples are consistent in the simulation results (cf. Fig. 5). Furthermore, the numerical and experimental results for scan velocities of $3.2 \frac{\text{m}}{\text{s}}$, $4.0 \frac{\text{m}}{\text{s}}$ and $6.4 \frac{\text{m}}{\text{s}}$ agree with each other. Small differences between numerical and experimental data are only found for $0.8 \frac{\text{m}}{\text{s}}$, $1.6 \frac{\text{m}}{\text{s}}$, $2.4 \frac{\text{m}}{\text{s}}$, $4.8 \frac{\text{m}}{\text{s}}$ and $5.6 \frac{\text{m}}{\text{s}}$ for higher line energies; for $v_{\text{scan}} = 0.8 \frac{\text{m}}{\text{s}}$ in experimental data swelling already occur for 0.4 and $0.5 \frac{\text{kJ}}{\text{m}}$ but in numerical data no swelling is measured. The same effect is seen for scan velocities 1.6 and $2.4 \frac{\text{m}}{\text{s}}$ where swelling occurs for smaller line energies experimentally than numerically. For higher scan velocities of 4.8 and $5.6 \frac{\text{m}}{\text{s}}$ the reverse effect is observed, i.e., more swelling occur numerically than experimentally. For $v_{\text{scan}} = 4.8 \frac{\text{m}}{\text{s}}$ swelling arises numerically already for a line energy of $0.25 \frac{\text{kJ}}{\text{m}}$ while the experimental setup is still good. The same is seen for $v_{\text{scan}} = 5.6 \frac{\text{m}}{\text{s}}$; line energies higher than $0.25 \frac{\text{kJ}}{\text{m}}$ lead to swelling in numerical simulations, but in experimental data only energies equal $0.3 \frac{\text{kJ}}{\text{m}}$ arise swelling.

^a<http://www.rrze.uni-erlangen.de/dienste/arbeiten-rechnen/hpc/systeme/lima-cluster.shtml>

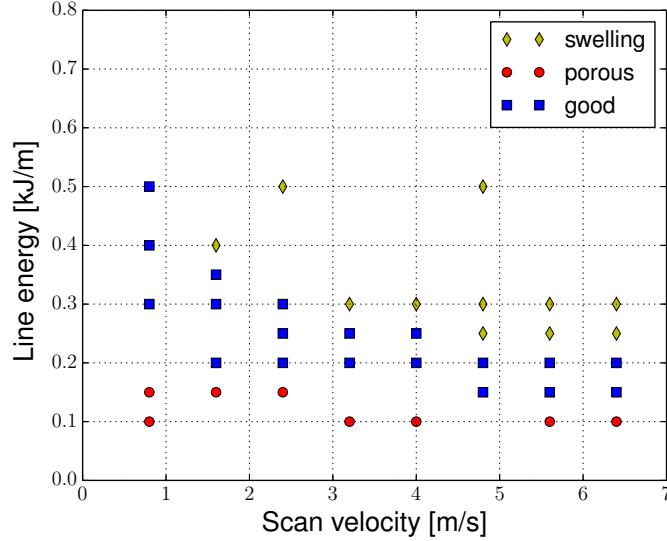


Fig. 5. Process window of numerical data. $\Delta x = 5 \cdot 10^{-6}$ m, $\Delta t = 1.75 \cdot 10^{-7}$ s, simulated powder domain $(1.44 \times 0.64 \times 0.24) \cdot 10^{-3}$ m³, beam offset = $13.56 \cdot 10^{-3}$ m.

Both effects can be explained by the focus of the electron beam gun. The focus is more precise for smaller scan velocities imposed by a smaller electron beam power P_{beam} , e.g. $v_{\text{scan}} = 1.6 \frac{\text{m}}{\text{s}}$ or $v_{\text{scan}} = 2.4 \frac{\text{m}}{\text{s}}$ lead to a precise, small focus and thus, energy is brought onto a smaller area. For these velocities swelling occurs for smaller line energies experimentally than numerically because the EB gun focus is constant for different beam power and scan velocities, respectively. For higher scan velocities (larger P_{beam}) like $4.8 \frac{\text{m}}{\text{s}}$ the focus of the gun spreads and, subsequently, the same amount of energy is brought into a larger area of powder particles and the maximum temperature is smaller. As a consequence in experimental data less swelling occurs for higher scan velocities (larger P_{beam}) than in numerical data.

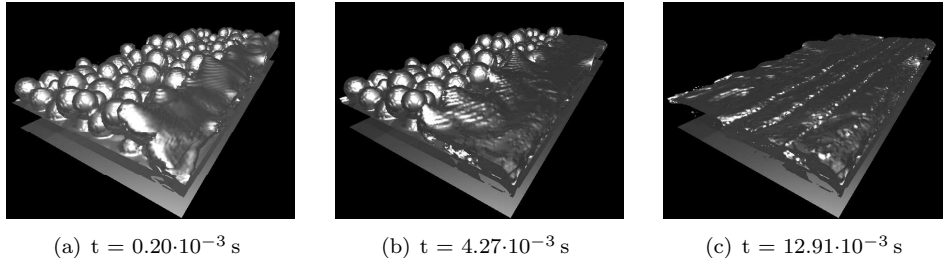


Fig. 6. Hatching of one layer, $(0.15 \frac{\text{kJ}}{\text{m}}, 6.4 \frac{\text{m}}{\text{s}})$.

Fig. 6 shows hatching of one line with parameter set $(0.15 \frac{\text{kJ}}{\text{m}}, 6.4 \frac{\text{m}}{\text{s}})$ for three different time steps. The inverse Gaussian distributed powder particles⁴ are demonstrated and the free surface is visualized by an isosurface. In Fig. 6(a) the electron beam melted one line and powder particles in this first line are not yet

8 Regina Ammer, Matthias Markl, Vera Jüchter, Carolin Körner, Ulrich Råde

completely melted. The next Fig. 6(b) shows the second melted line by a coming-back electron beam. Here, the particles of the first line are now melted completely. In the third Fig. 6(c) the electron beam has melted seven hatching lines and the whole powder layer is melted.

4. Conclusion

This paper describes the 3D thermal LB method for the numerical simulation of EBM processes. Experimental data of hatching a cuboid with different line energies and scan velocities are shown in a process window. The different samples are classified into porous, good and swelling, depending on the parameter set (line energy, scan velocity). For the validation all parameter sets are tested numerically and a numerical process window is generated by 3D simulations of hatching one powder layer. Numerical and experimental process window are highly concordant especially in the region of small line energies because parameter sets which are porous in experimental process window are that also in the numerical one. Only in the region between good and swelling differences exist which are reducible to the focus of the EB gun. The precision of the focus depends on the beam power but in our simulations the focus is constant.

In order to accelerate the building process of EBM manufacturing it is important to extend the process window, i.e., to raise up the question how the process window will look like for a higher beam power and therefore higher scan velocities. After the validation experiments in this paper which justify the correct behavior of our framework and its benefiting to simulate EBM processes we will try to find better parameter sets regarding quality of EBM products.

Acknowledgments

Our work is supported by the European Union Seventh Framework Program – Research for SME’s with full title “High Productivity Electron Beam Melting Additive Manufacturing Development for the Part Production Systems Market” and grant agreement number 286695. We also gratefully thank the German Research Foundation (DFG) for funding the experimental work within the Collaborative Research Centre 814, project B2.

References

1. P. Heintl et al., *Adv. Eng. Mater.* **9** 360 (2007).
2. C. Körner et al., *J. Mater. Process. Tech.* **211** 978 (2011).
3. M. Markl et al., *Procedia Comput. Sci.* **18** 2127 (2013).
4. R. Ammer et al., *Comput. Math. Appl.* **67** 318 (2014)
5. C. Feichtinger et al., *J. Comput. Sci.* **2** 105 (2011).
6. H. Köstler et al., *IT-Information Technology* **55** 91 (2013).
7. G.R. McNamara et al., *Phys. Rev. Lett.* **61** 2332 (1988).
8. U. Frisch et al., *Phys. Rev. Lett.* **56** 1505 (1986).

9. F. Higuera et al., *Europhys. Lett.* **9** 663 (1989)
10. F.J. Alexander et al., *Phys. Rev. E* **47** R2249 (1993)
11. Y. Chen et al., *Phys. Rev. E* **50** 2776 (1994)
12. F. Massaioli et al., *Europhys. Lett.* **21** 305 (1993)
13. X. Shan, *Phys. Rev. E* **55** 2780 (1997)
14. X. He et al., *J. Comput. Phys.* **146** 282 (1998).
15. P. Lallemand et al., *Int. J. Mod. Phys B* **17** 41 (2003)
16. G.R. McNamara et al., *J. Stat. Phys.* **81** 395 (1995).
17. P. Bhatnagar et al., *Phys. Rev.* **94** 511 (1954).
18. S. Chen et al., *Annu. Rev. Fluid Mech.* **30** 329 (1998).
19. X. He et al., *Phys. Rev. E* **56** 6811 (1997)
20. X. He et al., *Phys. Rev. E* **55** R6333 (1997)
21. C. Körner et al., *J. Stat. Physics* **121** 179 (2005).